Earth Systems, Resources, and Sustainability, 2026, 1(2), 183–201

Scilight

Earth Systems, Resources, and Sustainability

Journal Homepage: https://www.sciltp.com/journals/esrs

Article

Lower Vindhyan Succession as a Condensed Horizon in Central India

Gaurav K. Singh[1,*], Ashish K. Rai[1], Arif Husain Ansari[2] and Arvind K. Singh[3]

[1] Department of Applied Geology, Dr. Harisingh Gour Vishwavidyalaya, Sagar 470003, India
[2] Birbal Sahni Institute of Palaeosciences, Lucknow 226020, India
[3] Geological Survey of India, Shillong 793006, India
[*] Correspondence: letterstowest@gmail.com

ABSTRACT

Condensation is considered as a function of a sharp decline in sedimentation rate and accumulation of highly thin succession embracing a broad stratigraphic interval. Condensed sections are fairly common in various sedimentary basins and their investigation is important as they are regionally reliable marker horizons for sequence stratigraphic correlation. Elevated concentration of glauconite is essentially found confined to condensed sections. Throughout the earth's history, authigenesis driven glauconite genesis have been correlated with rising sea level and even interpreted as a manifestation of the 'Greenhouse' conditions. In ancient depositional systems as well, the occurrence of glauconite rich layers is often linked with marine flooding surfaces. Lower Vindhyan succession of Palaeoproterozoic age in central India constitutes one of the systems in which the presence of authigenic glauconite has been found associated with the stratigraphic condensation. These sediments often referred as Semri Group of rocks show glauconite rich layers in relatively thinner sections. The glauconite bearing condensed sections of Semri succession in central India has provided a regional correlation bench mark to trace basin wide unconformities for about 200 km. Here, we present the sequence stratigraphic framework of lower Vindhyan succession in Bundelkhand region around Hirapur for the first time.

ARTICLE INFO

History:

Received 25 December 2025
Revised 19 January 2026
Accepted 5 February 2026
Published: 6 March 2026

Keywords:

Hirapur;
glauconite;
condensed section;
Vindhyan;
sequence stratigraphy

Citation:

Singh, G.K.; Rai, A.K.; Ansari, A.H.; et al. Lower Vindhyan Succession as a Condensed Horizon in Central India. *Earth Systems, Resources, and Sustainability* **2026**, *1*(2), 183–201. https://doi.org/10.53941/esrs.2026.100012

Research Highlights

- Abnormally thin glauconite rich Proterozoic Lower Vindhyan succession (<25 m) has been traced for more than a hundred kilometres.
- They represent the case of condensed Semri deposits in the Bundelkhand region.
- The glauconites are mostly early diagenetic in nature.

1. Introduction

The Precambrian stratigraphic record encompasses a greater time interval and presents a unique opportunity to comprehend the sedimentary processes at a broader scale, and thus gaining an enhanced insight in to the facies cyclicity and the variability thereof [1]. Precambrian successions therefore offer a better understanding of some significant aspects of sequence stratigraphy, for which the time span of Phanerozoic, is too limited [2]. Several works have been published pertaining to the phanerozoic sequence stratigraphy perhaps due to its enormous application in the hydrocarbon exploration. Scarcity of well exposed sections, absence of age marker fossils and difficulty in dating allow only facies-based approach in the sequence stratigraphic analysis of the Precambrian succession. In the Indian subcontinent, Proterozoic sedimentary basins are not only well exposed, but are economically productive as well. The largest of these is the Vindhyan basin with shallow marine deposits possibly commencing from 1718 $\pm$ 94 Ma [3]. This succession is being explored for diamond reserves, cement and even hydrocarbon potential in Bundelkhand region of central India. Recently, the hydrocarbonsource rock potential of Vindhyan shales has also been attempted [4]. Commonly, Semri Group is referred as the Lower Vindhyan whereas other Groups are included under the Upper Vindhyan succession [5, 6]. The best fieldbased sedimentological work that documents depositional environment is by Singh and Kumar [3] and Singh [4]. Singh and Kumar [5] have regarded the Semri sediments around Chitrakut area as condensed deposits whereas the generalized sequence stratigraphy of Vindhyan basin is attempted by Bose et al. [7]. Some significant reports of microbially induced sedimentary structures, sedimentary processes and sea level fluctuations can be found in Sarkar et al. [8, 9]. Apart from the aforementioned contributions, no work exists that documents the presence of glauconite in response to the stratigraphic condensation and its application as a bench mark to delineate the basin wide unconformities. Until now, the Semri sequence around Bundelkhand craton (Figure 1) was largely unaddressed especially in terms of sequence stratigraphy. No documentation can be seen that combines diagenesis, field-basedobservation, and glauconite genesis.

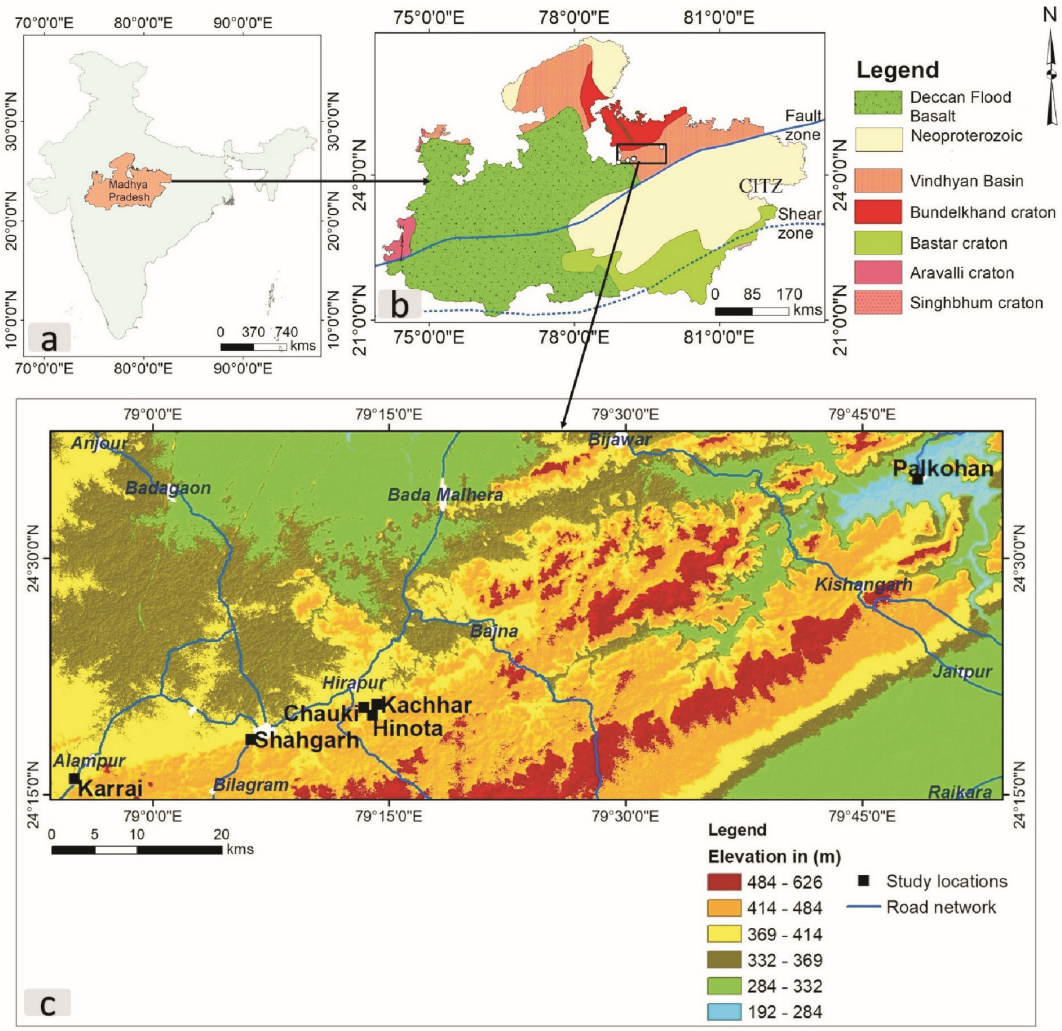

Figure 1. Geographic location map illustrating the study sites including Palkohan, Kachhar, Shahgarh and Karrai. Regional elevations have been marked with color.

In this work, the presence of prominent and considerably persistent glauconite horizon, diagenesis and the occurrence of syn-sedimentary concretions have also been reported. Such a multi-proxy approach establishes the condensed nature of the Semri sediments and provides a sequence stratigraphic framework to the Lower Vindhyan rocks for the first time from Bundelkhand region of the central India.

2. Material and Methods

Four sedimentary sections (Figure 2) were logged and sampled from different stratigraphic positions throughout the sandstone-shale-limestone succession to analyze the potential texture and composition through petrography and to study the genesis of glauconite. The stratigraphic thickness data from the four measured sections is applied to develop ageological model using the Groundwater Modelling System (GMS) software that included the thickness of individual strata, distances and angular relationships between sections. This data was processed to ensure consistency and accuracy, with methods applied to estimate any gaps or inconsistencies. It was then imported into GMS, where the software tools were used to define stratigraphic layers, position of the stratigraphic sections with respect to each other to construct cross sections between them and a 3D geological representation of the subsurface as well. The resulting model was validated through field observations to ensure its reliability.

20 samples (Table A1) were obtained from sandstones and shale of all the four sections for petrography, and X-ray-diffraction (XRD) have been studied. Glauconite bearing shales were analyzed for X-ray-diffraction (XRD). The texture of the rocks under thin-section along with the glauconite grains were studied first under binocular microscope for morphological characterization. During the petrographic study, several photomicrographs of the glauconite-bearing facies were taken with a camera connected to a petrographic CENSICO, model no. 13524 microscope. The structure of the silica matrix was examined by a Powder X-ray Diffraction (PXRD) Bruker XRD D-8 Advance 206890 for which copper was used as the cathode for generation of X-rays of wavelength (λ) = 1.54060 Å. Powder X-ray-diffraction (PXRD) diagrams from powder glauconite grain concentrates (reduced in size with an agate mortar) treated with ethylene glycol, were recorded using a Bruker XRD D-8 Advance 206890 for which copper was used as the cathode for generation of X-rays of wavelength (λ) = 1.54060 Å. Qualitative elemental analyses were also obtained through the aforementioned NOVA NANO SEM 450 SN 9921187 (SIC, DHSGSU), equipped with an energy-dispersive X-ray spectroscopy system (EDX).

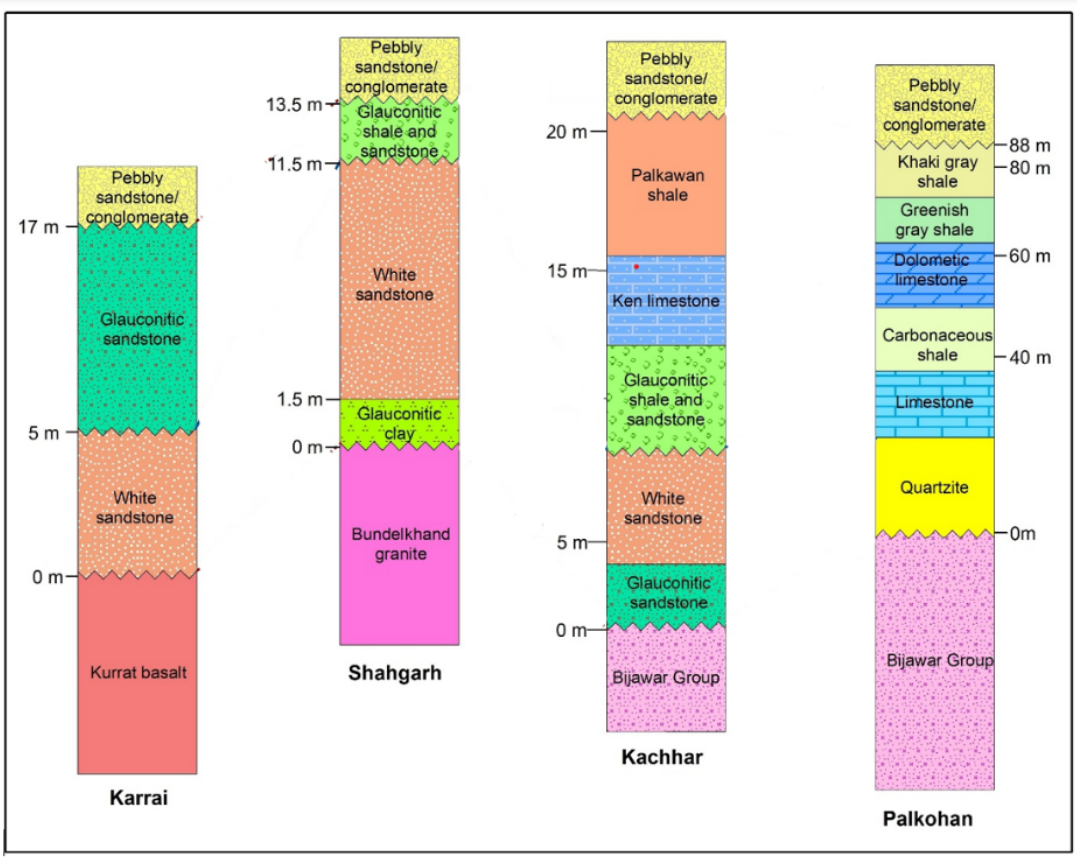

Figure 2. General litho-log of the Semri succession measured individually showing significant rock units in all the four sections.

3. Geological Background

The Vindhyan Supergroup non-conformably overlies the granitic/gneissic basement of the Archaean age and Paleoproterozoic Bijawar basin of Bundelkhand Craton. It comprises orthoquartzite-shale-carbonate association [6, 10] of about 4500 m [11] as a function of a delicate balance between accommodation space and net deposition [7]. The entire succession is divided in to four series later modified as Groups viz., Semri, Kaimur, Rewa and Bhander [12]. As noted above, these sediments rest unconformably over basement granites and early Proterozoic sediments with their interface marking a major basin wide unconformity. Another similarly significant unconformity divides the Vindhyan Supergroup in to Lower and Upper Vindhyan [13, 14]. The unconformity surface between Lower and Upper Vindhyan has been referred as a drop in sea level [7]. This unconformity is persistent all over the basin and is characterized by a decline in carbonate and predominance of siliciclastic rich sediments. It can therefore be said that the Lower Vindhyan (Semri) system is bounded by a major basement-cover unconformity at the base and by another major unconformity on the top at its contact with Kaimur Group of Upper Vindhyan sequence. Over about $\sim$80,000 km^2 of Vindhyan basin is covered by the Deccan Traps and, across an area of $\sim$10,000 km^2 at its northern fringe, by the Indo-Gangetic Plain [15]. Within the regional expanse of the exposed Vindhyan sediments, the succession here studied refers to the outcrops of the Lower Vindhyan rocks around Palkohan, Kachhar, Shahgarh and Karrai in Bundelkhand area, central India (Figure 1). The stratigraphic sections investigated in this work span a spatial distance of about more than two hundred kilometers from Palkohan in the northeast to Karrai towards southwest.

In the region around Hirapur (Figure 1), the basal layer which is predominantly sandstone is locally termed as Pandwafall Sandstone and forms the lowest unit of the Semri Group having Palaeoproterozoic age (Table A2). The average detrital zircon (U–Pb) age of 1718 $\pm$ 94 Ma [2] from the Pipartola conglomerate lying stratigraphically above the Palkawan Shale (Figure 2) and between Semri and Kaimur Group; provides the upper age limit of Semri sedimentation. In Son valley, the approximate age of the upper part of the Semri Group of rocks can be attributed to be about 1600 Ma [15]. This part is referred to as the Salkhan Limestone which has been considered as a part of Kheinjua Subgroup [16]. It means that Semri sedimentation has started earlier in Bundelkhand region and later in Son valley area reflecting the time-transgressive nature of the succession (Table A2) [5, 15, 17].

3.1. Facies Type Description

Facies characterization in this area is based primarily on the grain size and bedform, however, Singh and Kumar [5] and Singh [6] have done significant work on the depositional environment of Semri Group of rocks exposed elsewhere in the same basin. Overall, the facies association indicate an influence of tidal dominated process operated in a marginal marine environment. The depositional environment interpreted for the following group of facies is somewhat similar to the description given by Singh [6], however, with some differences.

4. Results

4.1. Facies Association

The lithology, grain size, primary sedimentary structures, horizontal-vertical relationships and the process have been considered as the basis for facies characterization, hence seven facies (Facies-A–G) are identified. Based on the similarity of most of these aforementioned parameters; the individual facies have been grouped in to following three associations.

4.1.1. Plane Laminated Glauconitic Facies

Facies-A exhibits fine grain, plane laminated character with a predominance of suspension driven process. They are exposed at Shahgarh and Kachhar and are glauconite rich.

4.1.2. Plane to Cross-laminated Sandstone Facies Association

Three facies viz. B, C and D have been merged together in this association of medium to coarse grained quartz arenites mainly driven by traction. They show small ripples, planar to tangential cross-lamination and even herringbone cross-stratification. These sediments are also characterized by synaresis cracks Figure 3(B2) and wedge shaped swash-backwash cross-stratification (Figure 4D).

4.1.3. Plane Laminated Limestone and Carbonaceous Mudstone Faciesassociation

Limestone dominated unit of Facies-E is combined with carbonaceous mudstone of Facies-F. Together, both the facies form a limestone-shale association. The limestone dominated succession is altogether absent in southwest and is exposed only towards northeast along Kachhar and Palkohan section. They do not exhibit any well-defined sedimentary structures except for planar even lamination (Figure 3E) and less frequent cross-lamination.

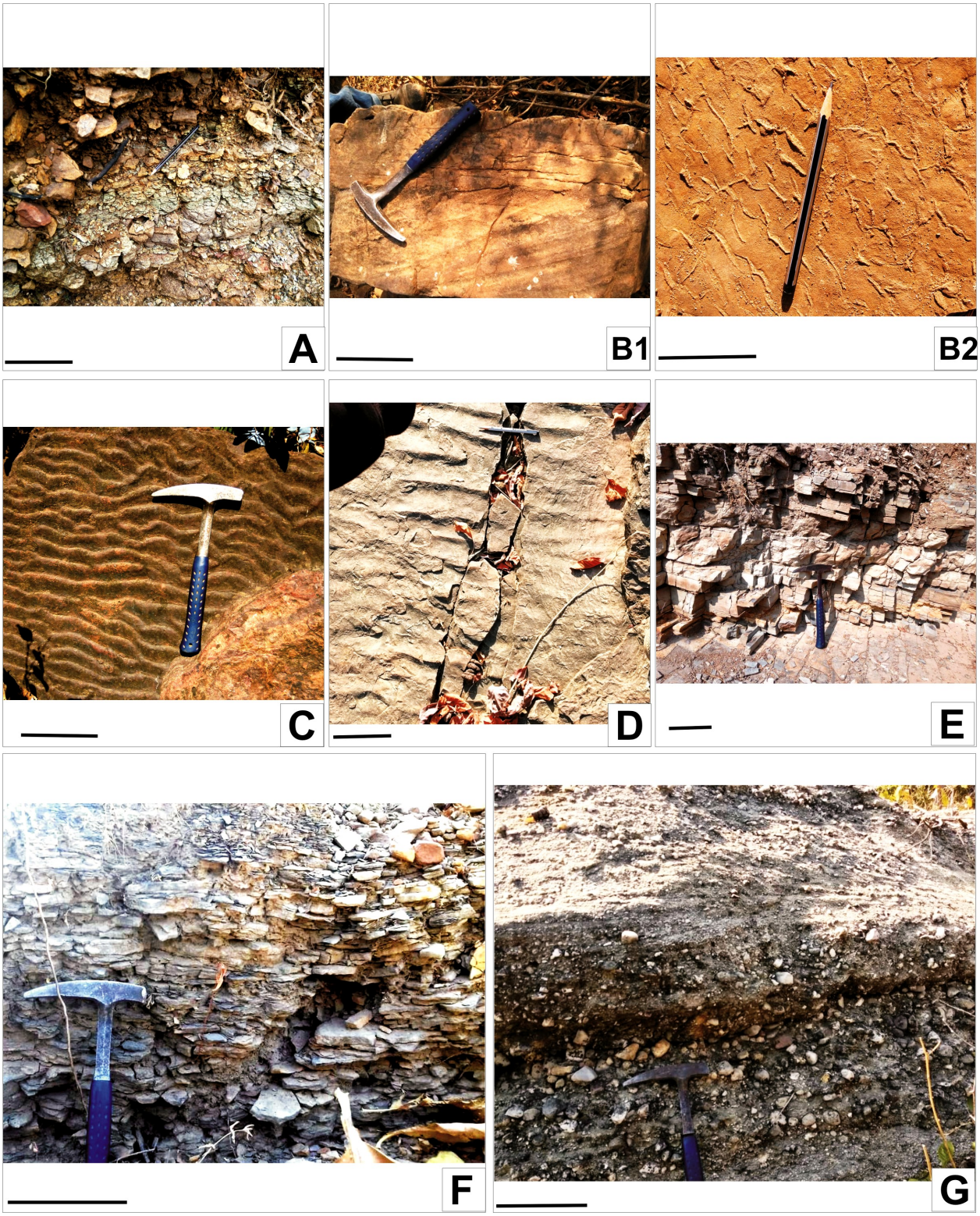

Figure 3. (**A**) Plane laminated glauconitic shale of facies-A exposed at Shahgarh (refer to panel-a of Figure 1 for location) scale bar: 12 cm; (**B1**) White sandstone (facies-B) exposed near Chauki showing bidirectional cross-stratification (refer to panel-b of Figure 1 for location) scale bar: 18 cm; (**B2**) Glauconitic sandstone (facies-B) exposed near Chauki showing syneresis cracks (refer to panel-b of Figure 1 for location) scale bar: 7 cm; (**C**) Rippled sandstone of facies-C near Chauki (refer to panel-b of Figure 1 for location) scale bar: 15 cm; (**D**) Nearly straight crested ripple on the sandstoneof facies-D exposed at Shahgarh (refer to Figure 1c for location) scale bar: 11 cm; (**E**) Plane laminated limestone of facies-E observed at Chauki (refer to Figure 1c for location) scale bar: 25 cm; (**F**) Thinly laminated shales of facies-F exposed at Palkohan (refer to Figure 1c for location) scale bar: 16 cm; (**G**) Monomictic conglomerate of facies-G near Shahgarh (refer to Figure 1c for location) scale bar: 32 cm.

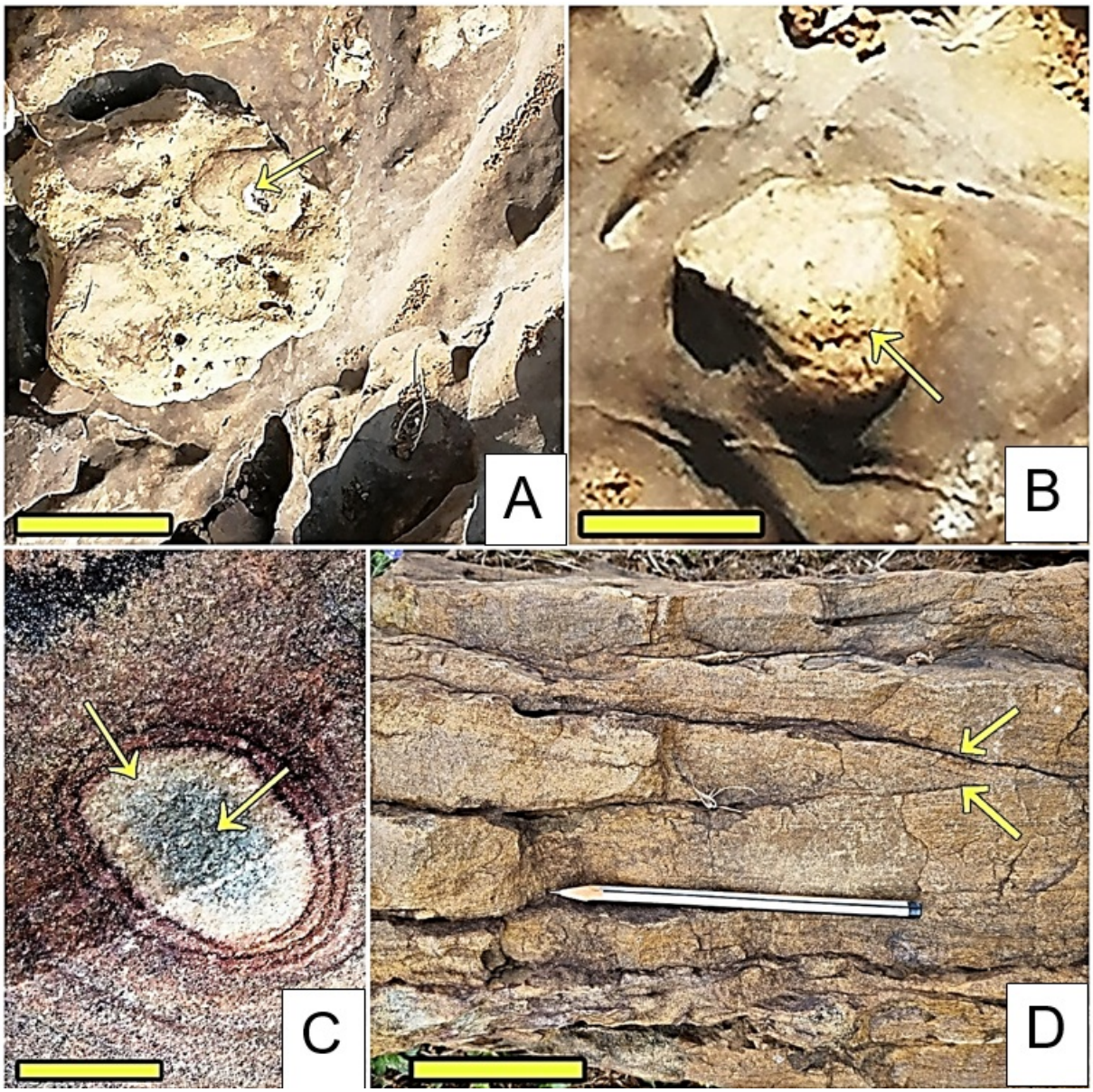

Figure 4. (**A**) Reworked concretions in a limestone exposure near Chauki composed of compound concretions (arrows) ofmoderate preservation quality (refer to Figure 1 for location); scale bar: 5 cm; (**B**) Calcareous non-reworked concretions (arrows) in Ken Limestone exposed near Chauki, (refer to Figure 1 for location); scale bar: 5 cm; (**C**) Sandstone showing the concentric zoning in the Liesegang rings seen at Kachhar (refer to Figure 1 for location); scale bar: 3 cm; (**D**) Sandstone with wedge shaped swash-backwash cross-stratification (horizontal arrow) exposed near Kachhar (refer to Figure 1 for location) scale bar: 5 cm.

4.2. Reworked Concretions in the Semri Sediments

Concretions preserved within the layers are significant in the reconstruction of time-intervals and events hardly documented by the sediments [18, 19]. These events constitute erosional and non-depositional phases and greatly facilitate the analysis of unconformity bounded successions. Layers rich in concretions are fairly common within the medium to fine-grained Proterozoic Semri sediments near Kachhar and Shahgarh. Usually, they consist of subrounded or irregular nodules in fine to medium sand and carbonate, about 2–7 cm in dimension. Hence, the host sediment varies in composition from carbonate rock mainly limestone to medium grained sandstone. Average lamina thickness is about 10cm and concretions occur about 100 cm apart. In a carbonate host, the concretions exhibit a conglomeratic fabric (Figure 4A) with fine grained carbonate matrix indicating that the concretions have been reworked (cf. [18]). Other concretions have a typically smooth surface and are composed of the same material (Figure 4B). Concretions in the sandstones are less frequent, yet are well-rounded, discordant with respect to the primary layering and bear a distinct concentric zoning in the form of Liesegang rings (Figure 4C). They are

commonly found associated with planar lamination. A rhythmic precipitation is observed as a banded pattern made up of alternating rings of sand and iron oxide.

Concretions are common almost in every stage of diagenesis [19] and reflect the times of reduced sedimentation or omission [20–22]. These concretions are sometimes exhumed as a result of prolonged omission and erosion after cementation. In the Semri sediments, reworked concretions locally occur within fine-grained sediments, being the only evidence of sedimentary omission and phases of reworking. Additionally, other concretions in Semri sediments which appear much like their matrix and do not have any complex conglomeratic fabric. They also reflect periods of reduced sedimentation or erosion, but did not undergo exhumation.

4.3. Glauconite Petrography

XRD analysis reveals the glauconitegrains within the sandstone and shale layers as glauconite with minor amounts of glauconite-smectite based on broad reflections at 1.51 Å (060, 33 $\bar{1}$), 2.6 Å (131), 3.3 Å (003), 4.5 Å (020), 5.0 Å (002), and 10 Å (001) (Figure 5). The basal 10 Å (001) reflection is not observed which probably reflects poor crystallinity or mixed-layer glauconite–smectite disorder. Distinct reflections at 3.6 Å (11 $\bar{2}$) and 3.1 Å (112), and a slightly wide XRD warp between 25° to 40° 2θ (Figure 5) indicate that the glauconite grains are mixtures of the 1M and 1 Md polytype structures, which correspond to ordered glauconite and disordered glauconite-smectite [23, 24]. The (060) reflection at 1.51 Å confirms the presence of 'glauconite' (cf. [25]). Besides glauconite-smectite, the major mineral components found into clay size fractions are quartz, alkali feldspar and kaolinite. As the sandstone-shale succession rests on the basement granites hence, the aforementioned mineral components can be attributed to the typical granite derived mineral assemblage. Kaolinite is generally a product of the hydrolysis of feldspar under warm and humid climate [26]. Therefore, such minerals indicate the feldspar dissolution dominantly through preferential leaching diffusion-controlled mechanism leading to the incongruent dissolution [26]. All these features are indicative of slightly evolvedglauconite (cf. [24, 27, 28]).

Chemically, most of the glauconite grains present K_2O contents averaging 2.88 wt% in Karrai, 5.57–2.68 wt% in Kachhar and 6.48–3.96 wt% in Shahgarh section (Table A4). It clearly indicates a lateral variation of the relative proportion of glauconite in Semri sediments. Mature glauconites have K_2O concentration of 6 wt% or more, hence, the values obtained for the aforementioned sections characterises nascent, slightly evolved glauconite, and evolved respectively (cf. [27]). The total Fe_2O_3 contents range from an average of 2.26 to a maximum of 18.11 wt% (Table A3), which shows the glauconites are Fe-poor. As the content of Fe_2O_3 is less, hence, glauconite affinity can be considered.The measured aluminium (Al), magnesium (Mg), and silicon (Si) contents (expressed as oxides) are 5.98–22.10 wt% Al_2O_3, 1.65–2.51 wt% MgO, and 15.9–86.09 wt% SiO_2, respectively. The calcium contents (1.64–32.41 wt% CaO only in Kachhar section) are generally low, as expected in mature glauconite [20] (Table A3, Appendix A). The variable composition of the glauconites in terms of relative weight percentage of major oxides, the absence of oxidized grain surfaces, the lobate form of the grains, and the presence of cracks in the pellets indicate the authigenic nature of the glauconites (cf. [29]).

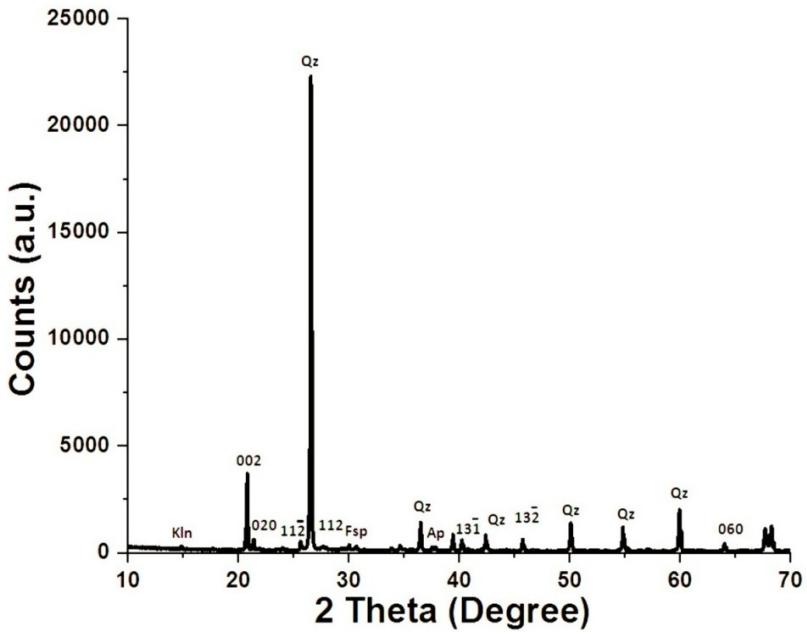

Figure 5. The X-ray diffractogram in random oriented glauconites in the glauconite-bearing sandstone and shale (sample nos. SHSH-1 and KASST-4) identifies (slight hump at $2\theta \sim 25°–40°$) ordered glauconite (1M polytype), disordered glauconite-smectite (1 Md polytype), quartz (Qz) and minor kaolinite (Kln), feldspar (Fsp), and apatite (Ap).

4.4. Petrography of the Sandstones

The modal composition based ternary plot (QFL) made (Figure 6, Table A4 in Appendix A) with Q (quartz), F (feldspar) and L (lithic fragments) based on Pettijohn [30]. It shows a quartz arenite affinity for all the sandstones of Semri Group studied in this work. Quartz is the predominant mineral phase with subordinate chert and K-feldspar grains. Quartz grains are rounded to sub-rounded and exhibit straight to slightly curved grain contact (Figure 7A). The framework grains have a pronounced overgrowth all around their margins (Figure 7A). At a few places, a partial or sometimes complete rim of glauconite is observed in between the detrital grain and the quartz overgrowth (Figure 7B). Glauconite content ranges between 15–20% of the sandstone. Other constituents including lithic fragments, polycrystalline quartz and chert content of the sandstone are in minor amounts (<5%). Under the microscope, glauconite commonly occurs as pellets representing pseudomorphic fills within a substrate which is so thoroughly altered without any evidence of its precursor. Based on the observed bulk mineralogy, quartz or feldspar may be the best possible substrate (Figure 7A). Additionally, there are pellets in which the substrate is partially altered and the relics of original substrate (algal cell) are preserved (Figure 7C). Besides them, glauconite also form a partial to complete rim of authigenic cement as mentioned above. Like the detrital clasts, the pellets are rounded to sub-rounded (Figure 7D) and are slightly finer than associated quartz and feldspar grains. They range in form from vermicular (Figure 7B), spheroidal (Figure 7C), and ovoidal forms (Figure 7D). Spherical glauconitehave diameter of about 30 µm, while long axis of capsular pellets (Figure 7D) up to 25 µm. The glauconite observed under plane polarized light is given in Figure 8A and B. Many of them exhibit cracks along margin of the pellets (Figure 9A).

As the glauconite intervenes between detrital quartz grain and syntaxial overgrowth, hence glauconite formed prior to the cementation possibly at initial diagenetic stages. With subsequent growth, the nucleating sites merged together engulfing almostthe entire substrate (Figure 9B). At an advanced stage, due to the pseudomorphic infilling, the glauconite occupies the space of a dissolved quartz grain leaving only a minor relict (Figure 9B). It therefore, documents pseudomorphic replacement of the quartz grains. As noted above, the most dominant mode of authigenic cementation consists of quartz as syntaxial overgrowth (Figures 8A and 9C). Another form of cement is the occurrence of quartz as passive pore-fill however, in minor amounts (Figure 9C). Syntaxial quartz overgrowth predates passive pore fill cements (Figure 9C) for which the detrital grains served as nucleation sites.

As the physical compaction of the sediments is followed by the chemical compaction [31] following soon after the mechanical compactionthereby enhancing porosity [32]. Enhanced porosity provides ample free space in the sediment to accommodate the authigenic growth of glauconite. In thin section, evidence of dissolution includes psudomorphic infilling by glauconite (Figure 9D). The replacement of the quartz grain along the margin by the glauconite (Figure 10) further supports the formation of glauconite by void-filling.The presence of relict glauconite cement between detrital grain and authigenic quartz overgrowth (Figure 7B) indicate the early diagenetic nature of glauconitization.

It is observed through petrography that the quartz cement as well as the glauconite was precipitated at an early stage in the burial history. Early quartz and glauconite authigenically precipitated from pore water forming coating on detrital quartz is more pronounced in intensity than the pseudomorphic infilling. Since the dominant pore filling cement is syntaxial; indicates the early diagenetic nature of the cementation (cf. [31]). During the early stages, the silica might have been derived from pore fluid circulating through the porous sand. In the later stage, pressure solution related to the framework-grain boundary contacts seems to have added additional silica to the pore fluids, which subsequently diffused to the other sites of precipitation. Since the grain contact is mostly straight to slightly curved and syntaxial overgrowth is the dominant mode of cementation hence, the sandstones are normal pressured reflecting slow sinking of the basin [31, 32].

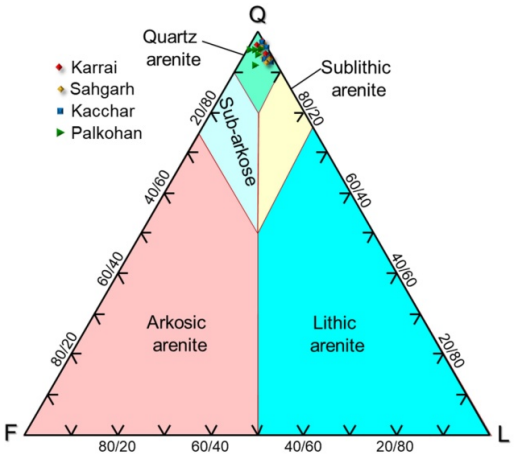

Figure 6. QFL diagram based on Pettijohn [30] plotted for Semri sandstones indicate that they are quartz-arenites.

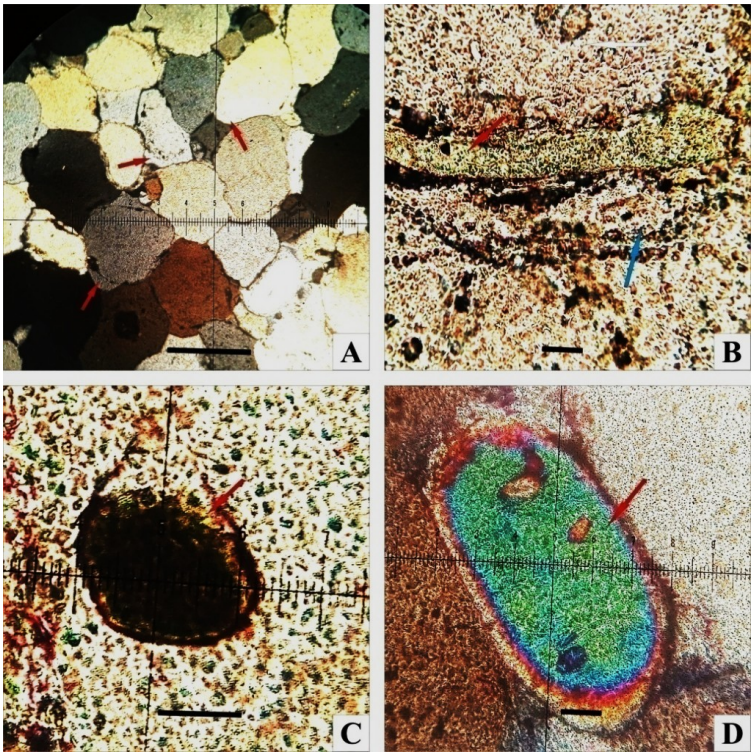

Figure 7. (**A**) Thin section photomicrograph of Pandwafall quartz arenite under thin section (XPL) showing rounded to sub rounded grains with syntaxial (arrows) authigenic silica cement (Scale bar: 10 µm). (**B**) A vermicular form (PPL) of glauconite (red arrow) occurring between detrital quartz (white arrow) and syntaxial overgrowth (blue arrow) (Scale bar: 2.5 µm). (**C**) An algal cell (PPL) infilled by glauconite (red arrow) (Scale bar: 10 µm). (**D**) Photomicrograph (XPL) showing a capsular pellet of the glauconite (scale bar: 2.5 µm).

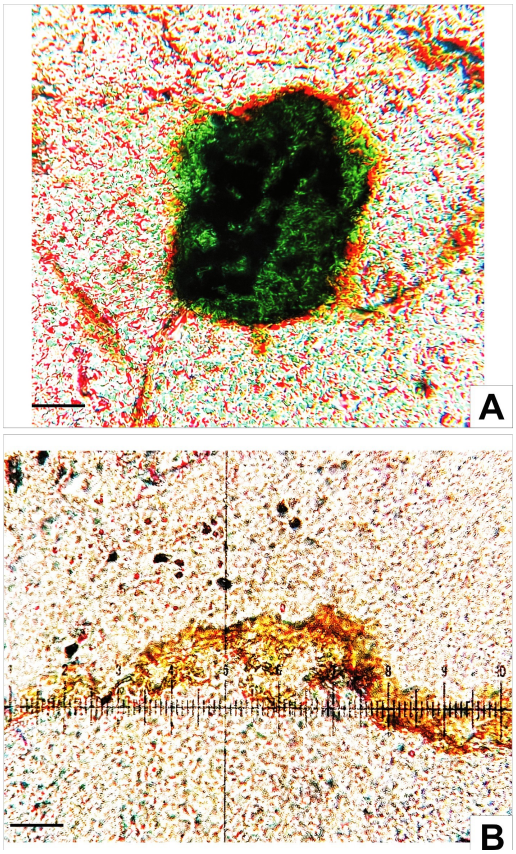

Figure 8. (**A,B**) Thin section photomicrograph of a green glauconite grain under plane polarized light (Scale bar: 10 µm).

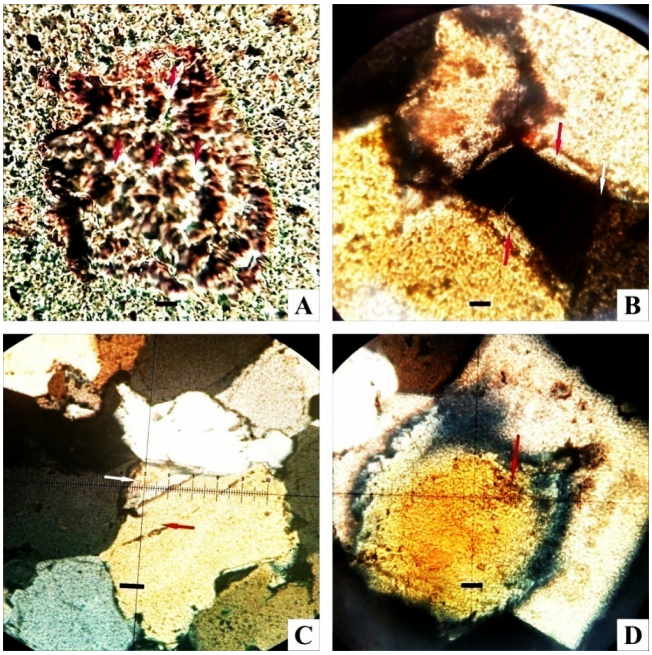

Figure 9. (**A**) Thin section photomicrograph of a glauconite grain (PPL) showing radially diverging cracks indicated by arrows (Scale bar: 2.5 µm). (**B**) Photomicrograph (XPL) showing relict quartz (red arrows) that survived glauconitization (white arrow) (Scale bar: 2.5 µm). (**C**) Photomicrograph (XPL) showing passive pore fill cement (white arrow) and red arrow indicates syntaxial quartz cement (scale bar: 10 µm) (**D**) Pseudomorphic infilling by glauconite (XPL) shown by the arrow (Scale bar: 2.5 µm).

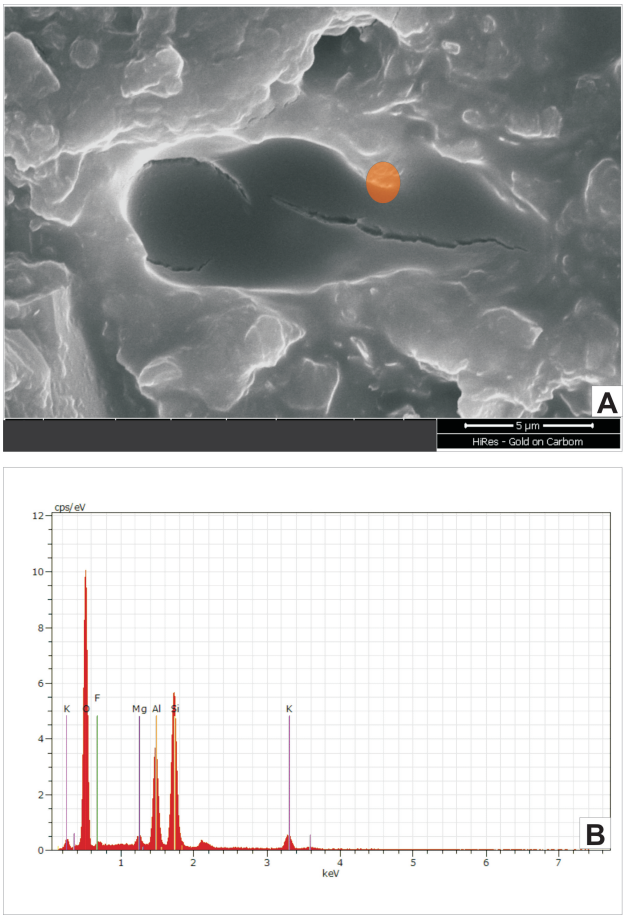

Figure 10. (**A**) Scanning Electron Microscopy (SEM) image of the Semri sandstone showing replacement of quartz by the glauconite. (**B**) The elemental graph of the spot highlighted with orange color in (**A**).

5. Discussion

A major part of the Vindhyan basin is aligned almost parallel to the Central Indian Tectonic Zone (CITZ) and is extended almost in WNW-ESE direction (Figure 1). The dominantly marine sediments were deposited in a nearly E-W trending basin with sea open towards west [13, 33]. Among them, the sediments of Semri Group in Bundelkhand region around Hirapur show a drastic thickness reduction from approximately 88 m in northeast to about 20–25 m towards southwest. Along with the reducing thickness, the succession shows a corresponding increase in the abundance of glauconite rich layers. As the highest accommodation space usually corresponds to the lower sedimentation rate reflected by glauconite rich layers towards shelf (cf. [34–37]), therefore the contention of westward opening of sea is further supported.

The most dominant host sediment of glauconite in Semri sediments in the area covered is sandstone serving as a porous substrate that favors the precipitation of glauconite (cf. [27]). The grain size of the glauconite pellets (20–30 µm) from the Semri sandstone is slightly coarser than associated detrital grains. Profuse quartz overgrowth around the quartz grains can be attributed to the available free space for the grain volume expansion exerted in the early diagenetic stage (cf. [38]). The presence of the glauconite cement between detrital grain and the quartz overgrowth (Figure 7B) indicate that its formation predates quartz cementation. Additionally, the presence of glauconite-smectite, an immature, iron rich precursor is also an indicative of an early diagenetic origin of the glauconite [35]. More mature, glauconite ($K_2O > 6$ wt%) showing later development have only been found in Shahgarh; whereas in all other sections however, the glauconites are immature and show early diagenetic affinity (Figure 11). Also, the presence of grain boundary fractures (Figure 9A) rules out any significant reworking (cf. [27, 35, 39]). As fossils are scarce in Precambrian sediments, the most suitable substrates for glauconite are feldspars, clay minerals and quartz grains. Only quartz (Figure 9B,D) and some algal cells (Figure 7C) can be identified as the original substrate, however, feldspars have been completely altered leaving no clue to its affinity. The alteration and replacement of quartz is observed from periphery towards the center (Figure 9D) somewhat similar to that demonstrated by Hughes and Whitehead [40]. In the present case, the precipitation and maturation of glauconite in a porous sandy substrate supports the 'verdissement theory' of Odin and Matter [27] with a major caveat being an extremely low value of Fe_2O_3. An overall low iron observed in the Semri sediments does not accord either with the "layer lattice theory" [38]. In present case, the pseudomorphic replacement theory seems more suitable to explain the genesis of these Precambrian glauconites in terms of negligible iron along with moderate contents of K_2O and Al_2O_3 [38, 41–46]. The little hump-like signal at $2\theta \sim 15^\circ$ (Figure 5) possibly indicates minor kaolinite polymorph which occurs as impurity (cf. [38]). Additionally, the ultimate basement of the Semri sediments is the granite which has the potential to provide ample K-feldspar. Through pseudomorphic replacement, it is also possible to explain the supply of excess K and Si in the pore-fluid by the dissolution of K-feldspar. A quartz dominated mineralogy and insignificant mafic minerals in the framework grains suggest that Fe and Mg contents in glauconite are sourced from the seawater. Such a form of the origin of secondary mineral glauconite by the replacement of unstable detrital grains viz. feldspar under sufficient geochemical constraints is interpreted to delineate unconformities that bound sequences [47, 48]. A shallow marine system with alkalinity of the sea water as a function of profuse continental chemical weathering detritus seems to be more suitable setting favoring the formation of glauconite. The MgO content in Semri sediments is moderate (1.64–2.5%) which accords with the Mg-rich Precambrian seas supporting glauconite genesis [42, 49]. The relatively moderate Al_2O_3 concentrations of glauconite is observed in almost all the sections studied (average $Al_2O_3 > 10\%$; Table A3) thus suggest shallow water depths (cf. [29]). Glauconite is typically found between 50–500 m of water depth and mostly concentrated around 200–300 m in modern oceans [27].

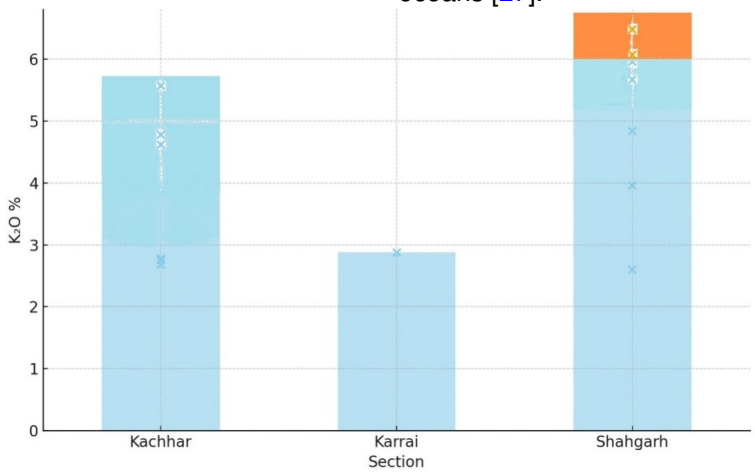

Figure 11. Histogram showing therelative proportion of the immature (blue) versus mature (orange) glauconite in the investigated sections. Immature glauconite is abundant.

Glauconite formation was favored in shallow marine settings in the Precambrian because of the availability of sandy sediments [38]. Low-Fe glauconite are usually formed under suboxic to oxic conditions in hypersaline lakes and lagoons [50, 51].

5.1. Facies and Glauconite based Sequence Stratigraphic Context of the Semri Sediments

In order to assign the depositional environment to the sedimentary profiles observed in the investigated area, the individual facies (Table A5) have been combined in to three facies associations (see Section 4.1). The first association has a single facies A and is made up of mostly fine-grained thinly laminated glauconitic shale, with thin sandy intercalations. They bear parallel lamination and the interlaminated minor sand layers show features indicating subaerial exposure e.g., raindrop imprints and syneresis cracks. Both the facies exhibit layers with a predominance of suspension driven process. The succession can be attributed to a lagoonal environment. Second association combines facies B,C and D and is predominantly made up of terrigenous clastic material often tens of meters thick. Generally, they constitute mainly sand admixed with minor mud layers. Bidirectional cross-stratifications Figure 3(B1) reveal intertidal setting, small channels and low angle discordances are common [6]. Facies C of this association can be laterally traced for hundreds of kilometers. Considering features indicating intermittent subaerial exposure, medium to fine sand composition and traction as the main process, a clastic tidal flat environment can be interpreted. The third association combines limestones of Facies-E with carbonaceous mudstones of Facies-F. The carbonate dominated succession do not exhibit any well-defined sedimentary structures except for planar lamination and less frequent cross-lamination, yet their association with tidal flat succession denotes a shallow marine origin. Overall, a carbonate tidal flat setting can be attributed to the Facies-E. Overall, the facies association indicate an influence of tidal dominated process operated in a marginal marine environment. The depositional environment interpreted for the following group of facies is somewhat similar to the description given by Singh [6], however, with some differences.

The base of tidally swept shallow marine Semri succession has been taken as the Transgressive Surface (TS) represented by a contact of these rocks with underlying granites or volcano-sedimentary Bijawar sediments (Figure 12A,B). These rocks lie over Bijawar succession for much more than 200 km and has a substantially reduced thickness compared to its depocenter in the Son valley area. At Shahgarh section, a thin band of glauconitic shale is interlaminated between these sandstones and the basement rocks. This layer contains about 50% of the slightly matured glauconite (with over 6 wt% K_2O) indicates a 'condensed surface' [52] hence, the Marine Flooding Surface (cf. MFS, [53–55]) lies just below this layer over the basement granites. A complete absence of any transgressive lag can be attributed to the subsidence well below the storm weather wave base (cf. [9]). The Transgressive Surface at Shahgarh section occurs over this glauconite rich layer. The entire sandstone succession lying over the Transgressive Surface (Figure 12A,B) have a persistent thickness of about 20 m for hundreds of kilometers and can be considered as Transgressive Systems Tract (cf. TST, [7, 56, 57]) which is commonly associated with significant sediment starvation [34, 58].

In Palkohan section, the MFS can be observed at the contact of basal whitish sandstone and overlying limestone (Figure 12A,B). Furthermore, at Palkohan section in the northeast direction, it is interesting to observe that the glauconite content is insignificant and there are two prominent bands of limestone-shale succession which gets reduced to just one band in Kachhar section with an increase in the glauconite rich layers. Towards southwest at Shahgarh section however, limestone-shale band is altogether absent (Figure 12A,B) and is marked with glauconitic shale and sandstones.It means that unconformity indicated by the glauconite rich layers towards southwest can be correlated to the limestone-shale rich succession in the northeast. Hence, facies based correlative conformity is interpreted towards northeast. In Karrai section further southwest, Semri Group gets reduced to a thickness of about 17 m with MFS interpreted at the base of glauconite rich sandstones (cf. [52, 53]). It can therefore be observed that from NE to SW, the aggregate thickness especially that of limestone-shale gets substantially reduced with a corresponding increase in the glauconite rich layers (Figure 12A,B). Such a feature reflects the deepening of the basin towards southwest. Also, the base of glauconite rich layers (cf. [53]) marking a Marine Flooding Surface and limestone-shale succession occurring towards northeast could possibly serve as the correlative conformity with maximum magnitude at the Palkohan section.

This study represents the first well-documented case of Proterozoic autochthonous, almost mature (slightly evolved; K_2O-rich ∼4–6 wt%, Table A3) glauconites of Semri sediments. Therefore, glauconite authigenesis is utilized here as a reliable indicator of reduced sedimentation along with reworked and non-reworked concretions possibly under dys-oxic depositional conditions (cf. [25]). Glauconite authigenesis thus marks the base of a transgressive condensed, tidal swept sequence deposited during the Proterozoic.

The present contribution provides a sequence stratigraphic framework to the Semri sediments around Hirapur along with a delineation of significant and basin wide sequence stratigraphic surfaces like Transgressive Surface (TS) and Marine Flooding Surface (MFS). As noted above, these surfaces mark regional level unconformities and their correlative conformity related to the stratigraphic condensation as a function of marine transgression. Enhanced accommodation space during transgression leads to a substantial condensation of the stratigraphic succession but the way it is linked with the changing geochemistry of the ocean and the connate pore fluid mainly manifested in the marine sediment record remains to be explored in future.

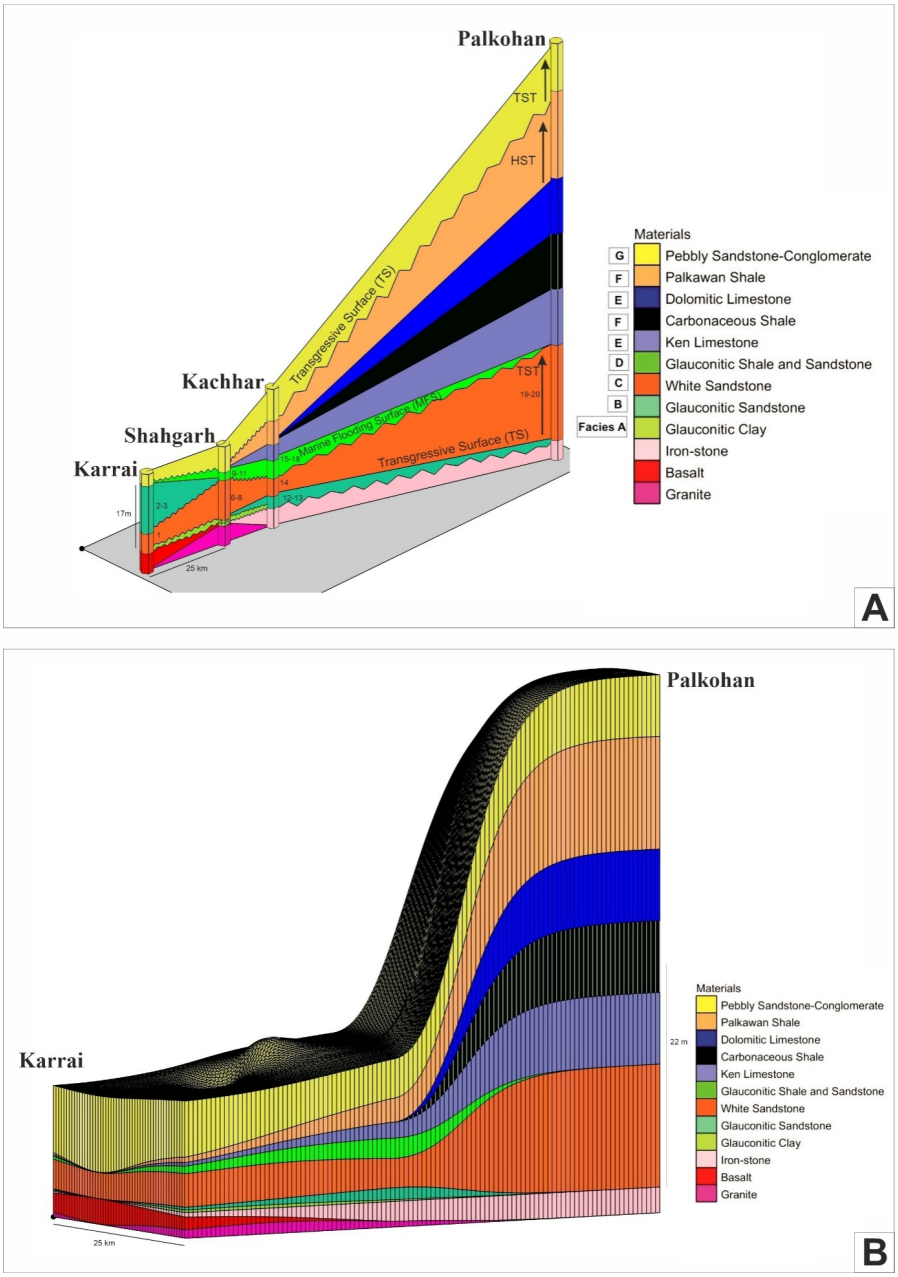

Figure 12. (**A**) General correlation log of the Semri succession showing significant stratigraphic surfaces and systems tract (TS = Transgressive Surface; MFS = Marine Flooding Surface; TST = Transgressive systems Tract; HST = High-stand Systems Tract). The facies designation is given in the capital letters and the sample serial numbers are marked on the individual sections (see Table A5 for details), (**B**) 3D model based on the measured stratigraphic data.

6. Conclusions

1. The lithostratigraphy of the Semri succession is established by envisaging the facies-based sequence stratigraphy in terms of the lateral lithological correlation of rock units. Hence, it provides a framework to compare ancient and modern facies-based sequence stratigraphic architecture.

2. The Semri Group of rocks in Bundelkhand region around Hirapur are condensed deposits formed in a tidal flat environment with the insignificant sedimentation rate and slow sinking of the basin.

3. The presence of syn-sedimentary concretions also indicates low sedimentation driven condensation. A well-developed section at Palkohan reflecting a limestone-shale rich correlative conformity with negligible glauconite content further supports this contention.

4. Glauconite formation is mostly early diagenetic in nature and corresponds with the quartz cementation.

5. Pseudomorphic replacement seems to be the most suitable mechanism by which the genesis of the glauconite in the Semri sediments can be explained.

Author Contributions

G.K.S.: Conceptualization, Methodology, Investigation, Original draft preparation, A.K.R.: Resources, Methodology, Investigation, A.H.A.: Resources, Methodology, Investigation, A.K.S.: Data curation. All authors have read and agreed to the published version of the manuscript.

Funding

This work has not received any financial support.

Institutional Review Board Statement

Not applicable.

Informed Consent Statement

Not applicable.

Data Availability Statement

All data generated or analyzed during this study are included in this published article.

Acknowledgements

We are extremely thankful to the two reviewers and the editors of the journal as their comments have greatly benefited to improve the manuscript. The authors also extend their gratitude to Arindam Gope, Atomic Mineral Division, New Delhi, India and Utkarsh Choubey for their cooperation in the field work. Pushpal Ghosh is especially thanked for making his XRD lab facility available for this work along with Satheesh C and his student Kundan for their participation in the finalization of the location map. We also extend our gratitude to Antareep Das for his help to prepare the fence diagram and useful discussion.

Conflicts of Interest

Authors declares that they have no conflicts of interest and no known financial or personal relationships that could have influenced the work reported in this paper.

Use of AI and AI-assisted Technologies

No AI tools were utilized for this paper.

Appendix A

Table A1. Details of samples along with the litho-units and locality (refer to Figure 2 for the stratigraphic position).

S. No.	Sample Identification No.	Rock Type	Location	Lat./Long.
1	KRSST-1	Sandstone	Karrai Section	Refer to Figure 1C, Karrai
2	KRSST-2	Glauconitic sandstone	Karrai Section	Refer to Figure 1C, Karrai
3	KRSST-3	Glauconitic sandstone	Karrai Section	Refer to Figure 1C, Karrai
4	SHSH-1	Glauconitic clay	Shahgarh Section	Refer to Figure 1C, Panel A
5	SHSH-2	Glauconitic clay	Shahgarh Section	Refer to Figure 1C, Panel A
6	SHSST-1	Sandstone	Shahgarh Section	Refer to Figure 1C, Panel A
7	SHSST-2	Sandstone	Shahgarh Section	Refer to Figure 1C, Panel A
8	SHSST-3	Sandstone	Shahgarh Section	Refer to Figure 1C, Panel A
9	SHSST-4	Glauconitic sandstone	Shahgarh Section	Refer to Figure 1C, Panel A
10	SHSH-3	Glauconitic clay	Shahgarh Section	Refer to Figure 1C, Panel A
11	SHSH-4	Glauconitic clay	Shahgarh Section	Refer to Figure 1C, Panel A
12	KASST-1	Glauconitic sandstone	Kachhar Section	Refer to Figure 1C, Panel B
13	KASST-2	Glauconitic sandstone	Kachhar Section	Refer to Figure 1C, Panel B
14	KASST-3	Sandstone	Kachhar Section	Refer to Figure 1C, Panel B
15	KASST-4	Glauconitic sandstone	Kachhar Section	Refer to Figure 1C, Panel B
16	KASH-1	Glauconitic shale	Kachhar Section	Refer to Figure 1C, Panel B
17	KASH-2	Glauconitic shale	Kachhar Section	Refer to Figure 1C, Panel B
18	KASH-3	Shale	Kachhar Section	Refer to Figure 1C, Panel B
19	PSST-1	Sandstone	Palkohan Section	Refer to Figure 1C, Panel C
20	PSST-2	Sandstone	Palkohan Section	Refer to Figure 1C, Panel C

Table A2. A comparative chart of the age of Semri succession [3, 15, 17].

Area	Group	Lithology	Chronostratigraphic Age
Son Valley	Semri	sandstone and Limestone	1600 Ma (11)
Hirapur (Bundelkhand)	Semri	Conglomerate and sandstone	1718 ± 94 Ma (2)

Table A3. Energy-dispersive X-ray (EDX) analysis of the glauconite displaying the semi-quantitative average K_2O, Al_2O_3 and Fe_2O_3 values (wt%).

Area	Sample-ID	$K_{\%}$	$K_2O\%$ = K%*1.2046	$Al_{\%}$	$Al_2O_{3\%}$= Al%*1.8895	Fe_2O_3	SiO_2	MgO	CaO
Karrai	KRSST-2	2.39	2.88	3.20	6.05	0.76	86.09	–	
Shahgarh	SHSST-4	5.05	6.09	11.59	21.90	2	51.56	1.98	–
	SHSH-2	5.05	6.09	11.15	21.07	2.14	55.4	2.03	–
	SHSH-1	5.37	6.48	11.70	22.10	1.66	57.47	1.83	–
	SHSH-3	4.94	5.96	11.16	21.09	1.84	57.32	1.73	–
	SHSH-4	4.37	5.27	9.71	18.35	2.87	52.38	1.99	–
	SHSST-1	3.28	3.96	9.18	17.35	2.63	46.3	2.1	1.66
	SHSST-2	4.01	4.84	9.73	18.39	2.74	50.62	2	–
	SHSST-3	2.15	2.60	7.14	17.28	3.26	35.8	1.8	6.68
Kachhar	KASH-3	2.28	2.75	6.33	11.97	–	75.59	1.7	11.9
	KASST-4	3.96	4.78	7.24	13.68	3.24	39.09	2.18	–
	KASH-1	3.83	4.62	9.43	17.82	2.10	54.02	2.51	2.37
	KASH-2	4.62	5.57	8.61	16.27	1.89	45.17	2.4	8.93
	KASST-2	2.23	2.68	3.16	5.98	–	15.9	2.11	32.6
	KASST-1	2.30	2.78	4.06	7.68	12.67	24.89	1.65	13.13

Table A4. Data recorded from the petrography of Semri sandstones.

S. No.	Locations	Quartz (%)	Feldspar (%)	Lithic Fragments (%)
1	Kr-1	92	2	6
2	Kr-2	94	1	5
3	Kr-3	96	2	2
4	Kr-4	93	1	6
5	Kr-5	97	0	3
6	S-1	93	1	6
7	S-2	95	2	3
8	S-3	96	1	3
9	S-4	92	2	6
10	S-5	97	0	3
11	S-6	96	1	3
12	S-7	93	2	5
13	S-8	94	1	5
14	Ka-1	97	0	3
15	Ka-2	96	0	4
16	Ka-3	93	1	6
17	Ka-4	94	1	5
18	Ka-5	93	2	5
19	Ka-6	92	1	7
20	P-1	95	3	2
21	P-2	95	4	1
22	P-3	94	3	3
23	P-4	91	5	4
24	P-5	95	3	2

Table A5. Individual facies description.

Facies	Grain Size	Sedimentary Structure	Top-bottom Relationship	Lateral Variation	Vertical Variation	Process
Facies-A	Fine grained glauconitic mudstone	Plane laminated (Figure 3A).	It lies over the basement granite and is overlained by sandstone with a rather sharp and abrupt contact.	Pinches out laterally, hence exposed only in Shahgarh section.	Very thin $<$2 m	Mostly suspension and fallout
Facies-B	Medium to fine grained glauconitic sandstone	Small, asymmetric, current ripples with sinuous crestsand planar to tangential Bidirectional cross-laminations Figure 3(B1), syneresis cracks Figure 3(B2).	It is disconformably situated over the ironstones at Kachhar section	Lateral persistence is limited.	Less than 5 m	Traction dominated
Facies-C	Medium to fine grained white sandstone	Structures same as Facies-B but without glauconite (Figure 3), syneresis cracks	At Palkohan, it is overlained by limestone while elsewhere; it is followed by glauconite rich sandstone and shales. The underlying lithology is Kurrat basalt in Karrai, granite in Shahgarh, ironstone in Kachhar and Palkohan section.	Highest lateral persistence, exposed in every section.	Variable between 5–20 m	Traction dominated
Facies-D	Alternation of fine-grained glauconitic sandstone and shale	Small, asymmetric current ripples and planar cross-laminations (Figure 3D)	At Kachhar, it is followed by limestone whereas elsewhere, it has a sharp contact with the pebbly sandstone. The underlying lithology is the sandstones of Facies-C	Persistent in every section except at Palkohan.	Ranges between 2–12 m	A combination of suspension, fallout and traction
Facies-E	Medium to fine grained limestone with shale intercalation	Mainly plane-laminated (Figure 3E) with minor current ripples and planar cross-laminations	It is followed by shales in both Kachhar and Palkohan section. The underlying lithology is sandstone in both the sections.	Exposed only at Kachhar and Palkohan section. Altogether absent towards northeast.	About 3 m thick at Kachhar whereas almost 30 m thick at Palkohan.	A combination of suspension and traction
Facies-F	Very fine-grained shale	Mainly plane-laminated (Figure 3F)	It is followed by pebbly sandstone or conglomerate in both Kachhar and Palkohan section. The underlying lithology is limestone of Facies-E in both the sections.	Exposed only at Kachhar and Palkohan section. Altogether absent towards northeast.	Approximately 5 m at Kachhar and more than 25 m at Palkohan.	Mainly suspension
Facies-G	Coarse to very coarse-grained granule stone or conglomerate	Planar to cross-laminated (Figure 3G)	The underlying lithology is variable from glauconitic sandstone at Karrai and Shahgarh to shales in Kachhar and Palkohan.	Persistent in every section	Varies from 5–20 m	High viscosity flow

References

1. Singh, A.K.; Chakraborty, P.P. Shales of Palaeo–Mesoproterozoic Vindhyan Basin, Central India: Insight into sedimentation dynamics of Proterozoic shelf. *Geol. Mag.* **2022**, *159*, 247–268.
2. Catuneanu, O.; Martins-Neto, M.A.; Eriksson, P.G. Precambrian sequence stratigraphy. *Sediment. Geol.* **2005**, *176*, 67–95.
3. Colleps, C.; McKenzie, N.; Sharma, M.; et al. Zircon and apatite U-Pb age constraints from the Bundelkhand craton and Proterozoic strata of central India: Insights into craton stabilization and subsequent basin evolution. *Precambrian Res.* **2021**, *362*, 106286.
4. Singh, A.K.; Chakraborty, P.P. Geochemistry and hydrocarbon source rock potential of shales from the Palaeo–Mesoproterozoic Vindhyan Supergroup, Central India. *Energy Geosci.* **2021**, *2*, 100073.
5. Singh, I.B.; Kumar, S. On the stratigraphy and sedimentation of the Vindhyan sediments in the Chitrakut area, Banda District (U.P.), Satna District (M.P.). *J. Geol. Soc. India* **1978**, *19*, 359–367.
6. Singh, I.B. Precambrian sedimentation sequences of India: Their peculiarities and comparison with modern sediments. *Precambrian Res.* **1980**, *12*, 411–436.
7. Bose, P.K.; Sarkar, S.; Chakrabarty, S.; et al. Overview of the meso- to neoproterozoic evolution of the Vindhyan Basin, central India. *Sediment. Geol.* **2001**, *141*, 395–419.
8. Sarkar, S.; Banerjee, S.; Chakraborty, S.; et al. Shelf storm flow dynamics: Insight from the Mesoproterozoic Rampur Shale, central India. *Sediment. Geol.* **2002**, *147*, 89–104.
9. Sarkar, S.; Banerjee, S.; Samanta, S.; et al. Microbial mat-induced sedimentary structures in siliciclastic sediments: Examples from the 1.6 Ga Chorhat Sandstone, Vindhyan Supergroup, M.P., India. *J. Earth Syst. Sci.* **2006**, *115*, 49–60.
10. Mandal, S.; Choudhuri, A.; Mondal, I.; et al. Revisiting the boundary between the Lower and Upper Vindhyan, Son Valley, India. *J. Earth Syst. Sci.* **2019**, *128*, 222–227.
11. Ahmad, F. Palaeogeography of central India. *Rec. Geol. Surv. India* **1958**, *87*, 530.
12. Auden, J.B. Vindhyan sedimentation in the Son Valley, Mirzapur District. *Rec. Geol. Surv. India* **1933**, *62*, 141–250.
13. Chanda, S.K.; Bhattacharya, A. Vindhyan sedimentation and paleogeography: Post-Auden developments. In *Geology of Vindhyachal*; Valdiya, K.S., Bhatia, S.B., Gaur, V.K., Eds.; Hindustan Publishing Corporation: Delhi, India, 1982; pp. 88–101.
14. Kwafo, S.; Meert, J.G.; Pandit, M.K.; et al. Searching for the age of upper Vindhyan Basin, India: A view from paleomagnetism and geochronology. *Geosci. Front.* **2026**, *17*, 102168.
15. McKenzie, N.R.; Hughes, N.C.; Myrow, P.M.; et al. New age constraints for the Proterozoic Aravalli–Delhi successions of India and their implications. *Precambrian Res.* **2013**, *238*, 120–128.
16. Sastry, M.V.A.; Moitra, A.K. Vindhyan stratigraphy: A review. *Mem. Geol. Surv. India* **1984**, *116*, 108–148.
17. Prasad, B.; Uniyal, S.N.; Asher, R. Organic-walled microfossils from the Proterozoic Vindhyan Supergroup of Son Valley, Madhya Pradesh, India. *Palaeobotanist* **2005**, *54*, 13–60.
18. Voigt, E. Uber Hiatus-Konkretionen. *Geol. Rundsch.* **1968**, *58*, 281–296.
19. Fürsich, F.T.; Oschmann, W.; Singh, I.B.; et al. Hardgrounds, reworked concretion levels and condensed horizons in the Jurassic of western India: Their significance for basin analysis. *J. Geol. Soc.* **1992**, *149*, 313–331.
20. Raiswell, R. Chemical model for the origin of minor limestone-shale cycles by anaerobic methane oxidation. *Geology* **1988**, *16*, 64–144.
21. Bathurst, R.G.C. *Carbonate Sediments and their Diagenesis*, 2nd ed.; Elsevier: Amsterdam, The Netherlands, 1975.
22. Fürsich, F.T. Genesis, environment and ecology of Jurassic hardgrounds. *Neues Jahrb. Geol. Palaontol. Abh.* **1979**, 158, 1–63.
23. Amorosi, A.; Sammartino, I.; Tateo, F. Evolution patterns of glauconite maturity: A mineralogical and geochemical approach. *Deep-Sea Res. II: Top. Stud. Oceanogr.* **2007**, *54*, 1364–1374.
24. Baldermann, A.; Banerjee, S.; Czuppon, G.; et al. Impact of green clay authigenesis on element sequestration in marine settings. *Nat. Commun.* **2022**, *13*, 1527.
25. Mandal, S.; Banerjee, S.; Sarkar, S.; et al. Origin and sequence stratigraphic implications of high-alumina glauconite within the Lower Quartzite, Vindhyan Supergroup. *Mar. Pet. Geol.* **2019**, *112*, 104040.
26. Yuan, G.; Cao, Y.; Schulz, H.M.; et al. A review of feldspar alteration and its geological significance in sedimentary basins: From shallow aquifers to deep hydrocarbon reservoirs. *Earth-Sci. Rev.* **2019**, *191*, 114–140.
27. Odin, G.S.; Matter, A. De glauconiarum origine. *Sedimentology* **1981**, *28*, 611–641.
28. Odin, G.S. *Green Marine Clays, Oolitic Ironstone Facies, Verdine Facies, Glauconite Facies, and Celadonite-Bearing Rock Facies: A Comparative Study*; Elsevier: Amsterdam, The Netherlands, 1988; p. 445.
29. Quirós, A.L.; Escutia, C.; Navas, A.S.; et al. Glauconite authigenesis, maturity and alteration in the Weddell Sea: An indicator of paleoenvironmental conditions before the onset of Antarctic glaciations. *Sci. Rep.* **2019**, *9*, 13580.
30. Pettijohn, F.J. *Sedimentary Rocks*, 3rd ed.; Harper & Row: New York, NY, USA, 1975; p. 628.
31. Worden, R.H.; Burley, S.D. *Sandstone Diagenesis: The Evolution of Sand to Stone*; International Association of Sedimentologists (IAS): Oxford, UK, 2003; pp. 3–44.
32. Singh, G.K.; Rai, A.K.; Singh, A.K. Diagenesis, facies and palaeocurrent analysis of Upper Rewa Sandstone around Sagar, central India. *J. Palaeogeogr.* **2023**, *12*, 546–563.
33. Banerjee, I. Barrier coastline sedimentation model and the Vindhyan example. *Q. J. Geol. Min. Metall. Soc. India* **1974**, *46*, 101–127.
34. Amorosi, A. Glauconite and sequence stratigraphy: A conceptual framework of distribution in siliciclastic sequences. *J. Sediment. Res.* **1995**, *65*, 419–425.
35. Amorosi, A. Detecting compositional, spatial, and temporal attributes of glauconite: A tool for provenance research. *Sediment. Geol.* **1997**, *109*, 135–153.
36. Berner, R.A. A new geochemical classification of sedimentary environments. *J. Sediment. Res.* **1981**, *51*, 339–365.
37. Odin, G.S. Significance of green particles (glauconite, berthierine, chlorite) in arenites. In *Provenance of Arenites*; Zuffa, G.G., Ed.; D. Reidel: Dordrecht, The Netherlands, 1985; pp. 279–307.
38. Banerjee, S.; Mondal, S.; Chakraborty, P.P.; et al. Distinctive compositional characteristics and evolutionary trend of Precambrian glauconite: Example from Bhalukona Formation, Chhattisgarh Basin, India. *Precambrian Res.* **2015**, *271*, 33–48.
39. Giresse, P.; Lamboy, M.; Odin, G.S. Evolution géométrique des supports de glauconitisation: Application á la reconstitution du paléoenvironnement. *Oceanol. Acta* **1980**, *3*, 251–260.
40. Hughes, A.D.; Whitehead, D. Glauconitization of detrital silica substrates in the Barton Formation (Upper Eocene) of the Hampshire Basin, southern England. *Sedimentology* **1987**, *34*, 825–835.
41. Dasgupta, S.; Chaudhuri, A.K.; Fukuoka, M. Compositional characteristics of glauconitic alterations of K-feldspar from India and their implications. *J. Sediment. Petrol.* **1990**, *60*, 277–281.
42. Banerjee, S.; Jeevankumar, S.; Eriksson, P.G. Mg-rich ferric illite in marine transgressive and highstand system tracts: Examples from the Palaeoproterozoic Semri Group, central India. *Precambrian Res.* **2008**, *162*, 212–226.
43. Banerjee, S.; Bansal, U.; Thorat, A.V. A review on palaeogeographic implications and temporal variation in glauconite composition. *J. Palaeogeogr.* **2016**, *5*, 43–71.
44. Banerjee, S.; Bansal, U.; Pande, K.; et al. Compositional variabil-

ity of glauconites within the upper cretaceous karai shale formation, Cauvery Basin, India: Implications for evaluation of stratigraphic condensation. *Sediment. Geol.* **2016**, *331*, 12–29.

45. Tang, D.; Shi, X.; Ma, J.; et al. Formation of shallow-water glauconite in weakly oxygenated Precambrian ocean: An example from the Mesoproterozoic Tieling Formation in North China. *Precambrian Res.* **2017**, *294*, 214–229.
46. Tang, D.; Shi, X.; Jiang, G.; et al. Ferruginous seawater facilitates the transformation of glauconite to chamosite: An example from the Mesoproterozoic Xiamaling Formation of North China. *Am. Mineral.* **2017**, *102*, 2317–2332.
47. Khalifa, M.A. Origin and occurrence of glauconite in the green sandstone associated with unconformity, Bahariya Oases, Western Desert, Egypt. *J. Afr. Earth Sci.* **1983**, *31*, 321–325.
48. Catuneanu, O. *Principles of Sequence Stratigraphy*; Elsevier: Amsterdam, The Netherlands, 2006; p. 375.
49. Harder, H. Syntheses of glauconite at surface temperatures. *Clays Clay Miner.* **1980**, *28*, 217–222.
50. Porrenga, D.H. Non-marine glauconitic illite in the Lower Oligocene of Aardebrug, Belgium. *Clay Miner.* **1968**, *7*, 421.
51. El Albani, A.; Meunier, A.; Fürsich, F.T. Unusual occurrence of glauconite in a shallow marine lagoonal environment. *Terra Nova* **2005**, *17*, 537–544.
52. Amorosi, A. The occurrence of glauconite in the stratigraphic record: Distribution patterns and sequence stratigraphic significance. In *Linking Diagenesis to Sequence Stratigraphy*; Morad, S., Ketzer, M., de Ros, L.F., Eds.; International Association of Sedimentologists Special Publication: Oxford, UK, 2013; Volume 45, pp. 37–53.
53. Amorosi, A.; Centineo, M.C. Anatomy of a condensed section: The Lower Cenomanian glauconite-rich deposits of Cap Blanc-Nez (Boulonnais, northern France). In *Marine Authigenesis: From Global to Microbial*; Glenn, C.R., Lucas, J., Lucas, L., Eds.; SEPM Special Publication: Tulsa, OK, USA, 2000; Volume 66, pp. 405–413.
54. Galloway, W.E. Paleogene depositional episodes, genetic stratigraphic sequences, and sediment accumulation rates, NW Gulf of Mexico Basin. In *Sequence Stratigraphy as an Exploration Tool: Concepts and Practices in the Gulf Coast*; SEPM Society for Sedimentary Geology: Claremore, OK, USA, 1991; pp. 165–176.
55. Sangree, J.B.; Vail, P.R.; Mitchum, R.M., Jr. A summary of exploration applications of sequence stratigraphy. In *Sequence Stratigraphy as an Exploration Tool: Concepts and Practices in the Gulf Coast*; SEPM Society for Sedimentary Geology: Claremore, OK, USA, 1991; pp. 321–327.
56. Sonnenfeld, M.D. Sequence evolution and hierarchy within the Lower Mississippian Madison Limestone of Wyoming. In *Paleozoic Systems of the Rocky Mountain Region*; Longman, M.W., Sonnenfeld, M.D., Eds.; SEPM Rocky Mountain Section: Tulsa, OK, USA, 1996; pp. 1–28.
57. Giles, K.A.; Bocko, M.; Lowton, T.F. Stacked Late Devonian lowstand shorelines and their relation to tectonic subsidence at the Cordilleran hingeline, western Utah. *J. Sediment. Res.* **1999**, *69*, 1181–1190.
58. Catuneanu, O.; Abreu, V.; Bhattacharya, J.P.; et al. Towards the standardization of sequence stratigraphy. *Earth-Sci. Rev.* **2009**, *92*, 1–33.